A&A 408, 601–610 (2003)
DOI: 10.1051/0004-6361:20030795

Astronomy & Astrophysics

Multiple outflows in IRAS 19410+2336⋆

H. Beuther[1,2], P. Schilke[1], and T. Stanke[1]

[1] Max-Planck-Institut für Radioastronomie, Auf dem Hügel 69, 53121 Bonn, Germany
[2] Harvard-Smithsonian Center for Astrophysics, 60 Garden Street, Cambridge, MA 02138, USA

Received 24 March 2003 / Accepted 16 May 2003

Abstract. Plateau de Bure Interferometer high-spatial resolution CO observations combined with near-infrared H_2 data disentangle at least seven (possibly even nine) molecular outflows in the massive star-forming region IRAS 19410+2336. Position–velocity diagrams of the outflows reveal Hubble-like relationships similar to outflows driven by low-mass objects. Estimated accretion rates are of the order of $10^{-4}\,M_\odot\,\mathrm{yr}^{-1}$, sufficiently high to overcome the radiation pressure and form massive stars via disk-mediated accretion processes. The single-dish large-scale mm continuum cores fragment into several compact condensations at the higher spatial resolution of the PdBI which is expected due to the clustering in massive star formation. While single-dish data give a simplified picture of the source, sufficiently high spatial resolution resolves the structures into outflows resembling those of low-mass star-forming cores. We interpret this as further support for the hypothesis that massive stars do form via disk-accretion processes similar to low-mass stars.

Key words. accretion, accretion disks – stars: early type – stars: formation – ISM: jets and outflows

1. Introduction

The physical processes forming massive stars are still subject to great debate. Basic low-mass star-forming theories predict small accretion rates independent of mass (10^{-6}–$10^{-5}\,M_\odot\,\mathrm{yr}^{-1}$, Shu 1977), which are not sufficient to overcome the radiation pressure of a star $\geq 8\,M_\odot$. More massive stars should not form according to that picture (Wolfire & Cassinelli 1987) although they are observed to exist. Several theories have been put forward to solve this discrepancy: if the standard scenario is adapted, higher accretion rates must be present and the accretion is likely to be mediated through disks (e.g., Wolfire & Cassinelli 1987; Jijina & Adams 1996; Norberg & Maeder 2000; Maeder & Behrend 2002; Yorke & Sonnhalter 2002; McKee & Tan 2003). Another scenario suggests that the very center of the evolving cluster is dense enough that intermediate-mass protostars collide, merge, and form the most massive objects via these collisions (e.g., Bonnell et al. 1998; Stahler et al. 2000; Bally 2002; Zinnecker & Bate 2002).

As high-mass star-forming regions are on the average far away (a few kpc) and massive stars form in a clustered mode, it is nearly impossible to resolve with current telescopes the forming cluster in the mm and sub-mm regime, and thus to study the physical processes forming the stars in a direct way. Infrared observations give ambiguous results at best, since the centers of activity are very deeply embedded and block out all infrared light, except in rare favorable geometries. Therefore, indirect approaches have to be taken. Massive molecular outflows are perfectly suited for such investigations, because outflows are observed on large spatial scales (in the parsec regime), they are easier to resolve spatially, and their structure and energetics give information on the physical processes close to their driving center. For example, the accretion scenario predicts outflows which are morphologically similar to low-mass outflows and which show a high degree of collimation due to the star-disk interaction (Richer et al. 2000). On the contrary, colliding protostars are expected to be extremely eruptive phenomena during which accretion disks should not be able to survive, and therefore the outflows are likely less collimated and rather resemble explosions as observed in Orion KL (Schultz et al. 1999).

Over recent years several single-dish studies of massive outflows have been undertaken (e.g., Shepherd & Churchwell 1996; Ridge & Moore 2001; Zhang et al. 2001; Beuther et al. 2002b). While these studies agree on the facts that outflows are ubiquitous phenomena in massive star formation and that they are very massive and energetic, there is considerable disagreement on the typical collimation of the observed outflows. Shepherd & Churchwell (1996) and Ridge & Moore (2001) claim that the average collimation of massive outflows is lower than observed for their low-mass counterparts supporting the proposal that massive star formation has to proceed through

Send offprint requests to: H. Beuther,
e-mail: hbeuther@cfa.harvard.edu

⋆ Based on observations with the IRAM Plateau de Bure Interferometer, the Calar Alto 3.5 m telescope and the IRAM 30 m. IRAM is supported by INSU/CNRS (France), MPG (Germany), and IGN (Spain). Calar Alto is operated by the MPIA in Heidelberg, jointly with the Spanish National Commission for Astronomy.

different physical processes such as coalescence. Beuther et al. (2002b) also observed lower collimation of massive outflows compared to low-mass sources. However, taking properly into account the poor spatial resolution, they argue that their data are well consistent with highly collimated outflows in high-mass star-forming regions (but proof of this requires interferometer observations). Thus, no other physical processes have to be invoked, and high-mass star formation can proceed as in the classical low-mass scenario, just with significantly enhanced accretion rates.

Despite the great advances during recent years, single-dish observations are not sufficient to understand the complex outflows in massive star formation. As always clusters of stars form simultaneously, it is likely that at high spatial resolution many of the single-dish outflows resolve into multiple outflows emanating from the same large scale core but from different protostars within them. Using Plateau de Bure interferometric observations Beuther et al. (2002d) showed that the chaotic single-dish outflow in IRAS 05358+3543 resolves into at least three molecular outflows at a spatial resolution of ∼3.5″. One of these outflows shows a collimation degree of 10, the highest so far observed in massive star-forming regions, and as high as the highest values known for low-mass star formation. The observations indicate that high-mass regions are more complex due to the clustered mode of formation, but that the physical processes taking place are similar to those of their low-mass counterparts.

There do exist other interferometric observations of high-mass outflows, e.g., IRAS 20126+2104 (Cesaroni et al. 1997; Shepherd et al. 2000), G192.16 (Shepherd et al. 1998), G35.2 (Gibb et al. 2003), but they are either covering only the very inner region not tracing the large scale outflow, or the spatial resolution does not exceed 5″.

In order to base the results obtained so far on a larger statistical base and observe more massive outflows at adequate high spatial resolution, we perform a series of high-resolution observations using the Plateau de Bure Interferometer (PdBI) and BIMA. Here, we present the results of PdBI observations of the outflow system in IRAS 19410+2336 which is part of a sample of 69 high-mass protostellar objects (HMPOs) studied over recent years in great detail (Sridharan et al. 2002; Beuther et al. 2002a–c). At the very center of the southern core, we detect H_2O and CH_3OH maser emission as well as a weak 1 mJy unresolved cm continuum source at a spatial resolution of 0.7″ (see Fig. 1). Assuming the latter to be due to optically thin free-free emission at 3.6 cm, it indicates a recently ignited but not very evolved massive object at the cluster center (Beuther et al. 2002c; Sridharan et al. 2002). It is also the most deeply embedded massive star-forming region which was ever observed with the *CHANDRA* X-ray satellite (Beuther et al. 2002e). So far, we only knew the kinematic distances which suffer from a distance ambiguity (Sridharan et al. 2002), but based on the new MSX and 2MASS data of the region we believe the near kinematic distance to be more likely (Bontemps, priv. comm.). Further on, we assume IRAS 19410+2336 to be at a distance of ∼2.1 kpc. The approximate bolometric luminosity of the region is $10^4\,L_\odot$. Single-dish 1.2 mm continuum observation reveal two massive adjacent dust cores, each associated with a bipolar molecular outflow as observed in CO(2–1) with 11″ resolution (Fig. 1, Beuther et al. 2002a,b). The single-dish data suggest a simple morphology in both cores which makes the region a good candidate for further studies of collimated outflows. The PdBI observations will show that the single-dish observations provide only a simplified picture of the real outflow structure.

2. Observations

2.1. Plateau de Bure Interferometer (PdBI)

We observed IRAS 19410+2336 in Summer 2001 with the Plateau de Bure Interferometer at 2.6 mm in the D (with 4 antennas) and C (with 5 antennas) configuration (Guilloteau et al. 1992). The simultaneously observed 1 mm data were only used for phase corrections because of the poor Summer weather conditions. The 3 mm receivers were tuned to 115.27 GHz (USB) (centered at the ^{12}CO 1 → 0 line) with a sideband rejection of about 5 dB. At this frequency, the typical SSB system temperature is 300 to 400 K, and the phase noise was below 30°. The frequency resolution at 115 GHz was 0.1 km s^{-1}, but we smoothed the data to 1 km s^{-1} which is sufficient to map the broad line wings. Atmospheric phase correction based on the 1.3 mm total power was applied. For continuum measurements, we placed two 320 MHz correlator units in the band to cover the largest possible bandwidths. Temporal fluctuations of the amplitude and phase were calibrated with frequent observations of the quasars 1923+210 and 2023+336. The amplitude scale was derived from measurements of MWC 349 and CRL 618, and we estimate the final flux density accuracy to be ∼15%. To cover both cores a mosaic of 10 fields was observed. We obtain a 3σ continuum rms of ∼5 mJy. The continuum data are already presented by Beuther et al. (2002e).

2.2. Short spacings with the IRAM 30 m telescope

To account for the missing short spacings and to recover the line-flux, we also observed the source in CO(1–0) with the IRAM 30 m telescope in Summer 2002. The observations were done remotely from Bonn in the on-the-fly mode. Due to previous software changes the online velocity correction was missing a term corresponding to some part of the earth rotation. This error was corrected offline by the AoD Gabriel Paubert. The velocity is estimated to be correct within 0.1 km s^{-1}.

The algorithm to derive visibilities from the single-dish data corresponding to each pointing center is described by Gueth et al. (1996). The single-dish and interferometer visibilities are subsequently processed together. Relative weighting has been chosen to minimize the negative side-lobes in the resulting dirty beam while keeping the highest angular resolution possible. Images were produced using natural weighting, then a CLEAN-based deconvolution of the mosaic was performed. The final beam size of the 2.6 mm data is 3.9″ × 3.6″ (PA 33°).

2.3. Calar Alto

The near-infrared camera Omega Prime on the 3.5 m telescope on Calar Alto/Spain was used to obtain 2.12 μm

Table 1. The mm sub-sources: positions, peak fluxes, integrated fluxes, derived core masses and column densities.

Source	RA	Dec	Flux	Peak	M	N_{H_2}
	[J2000.0]	[J2000.0]	[mJy]	[mJy/beam]	[$M_\odot$]	[10^{24} cm^{-2}]
mm1	19:43:11.24	23:44:03.4	29	19	83	2
mm2	19:43:11.17	23:44:07.4	39	19	112	2
mm3	19:43:10.59	23:44:01.5	14	9	40	1
mm4	19:43:11.17	23:43:48.0	13	8	37	1
mm5	19:43:10.68	23:44:58.4	10	8	29	1
mm6	19:43:10.81	23:45:07.0	13	8	37	1

narrow band H_2 and K' wide field images of the region around IRAS 19410+2336 on June 11, 2001. At a pixel scale of 0.4″ pixel^{-1}, the 1024 × 1024 pixel array provides a field-of-view of ∼6.″8 × 6.″8. The basic data reduction has already been described in Beuther et al. (2002e). The narrow-band line mosaic and the K' mosaic were then carefully registered. The Point Spread Function (PSF) of the H_2 image was degraded to match the PSF of the K' image with the poorer seeing; finally, the continuum image was scaled such that stars had the same flux as in the narrow band image. This image was then subtracted from the (PSF-degraded) narrow band image in order to provide the continuum subtracted narrow band image (see Fig. 3 for the K' and H_2 image).

3. Results

3.1. Millimeter continuum sources

The large-scale southern single-dish core splits into at least four sub-cores in the 2.6 mm continuum (Fig. 1), whereas the northern core is resolved into 2 sub-sources in the higher-resolution data. Assuming that the 2.6 mm continuum is produced by optically thin thermal dust emission, we can calculate the masses and the column densities of the different sub-cores following Hildebrand (1983):

$$M_{H_2} = \frac{1.3\times10^{-3}}{J_\nu(T)}\frac{a}{0.1\,\mu\mathrm{m}}\frac{\rho}{3\,\mathrm{g\,cm^{-3}}}\frac{R}{100}\frac{F_\nu}{\mathrm{Jy}} \times\left(\frac{D}{\mathrm{kpc}}\right)^2\left(\frac{\nu}{2.4\,\mathrm{THz}}\right)^{-3-\beta}\,[M_\odot]$$

$$N_{H_2} = \frac{7.8\times10^{10}}{J_\nu(T)\Omega}\frac{a}{0.1\,\mu\mathrm{m}}\frac{\rho}{3\,\mathrm{g\,cm^{-3}}}\frac{R}{100}\frac{F_\nu}{\mathrm{Jy}} \times\left(\frac{\nu}{2.4\,\mathrm{THz}}\right)^{-3-\beta}\,[\mathrm{cm^{-2}}]$$

where $J_\nu(T) = [\exp(h\nu/kT) - 1]^{-1}$ and Ω, a, ρ, R, and β are the beam solid angle, grain size, grain mass density, gas-to-dust ratio, and grain emissivity index for which we use the values 3.9″ × 3.6″ in radians, 0.1 μm, 3 g cm^{-3}, 100, and 2, respectively (Hunter et al. 2000). Based on IRAS far-infrared data, the dust temperature T is estimated to be around 46 K. As discussed by Beuther et al. (2002a), higher dust opacity indices (corresponding to a lower β) would result in lower masses and column densities whereas lower temperatures would increase the derived parameters. We estimate the results to be correct within a factor 5.

The masses range between 30 and 110 $M_\odot$ and the column densities are in the 10^{24} cm^{-3} regime, corresponding to a visual extinction of $A_v \sim 1000$ (see Table 1). The mm sources mm1 and mm2 are of similar mass but the most prominent sub-core is mm1, which coincides with the H_2O and CH_3OH masers and also with the weak cm continuum source (Beuther et al. 2002e). The continuum 3σ rms is ∼5 mJy equal to a mass sensitivity >14 $M_\odot$ at a temperature of 46 K. Assuming an $S_\nu \propto \nu^4$ relationship (i.e., $\beta = 2$) for the continuum dust emission in the mm regime, we compare the single-dish flux at 1.2 mm with the PdBI data at 2.6 mm and find that approximately 60% of the total continuum flux is filtered out by the interferometric observations. This most likely corresponds to emission from the large-scale envelope of the core, whereas the PdBI detected mm emission traces the very dense and compact condensations. As the weak 1 mJy cm continuum emission is most likely due to optically thin free-free emission, its contribution in the mm-regime is neglectable.

3.2. Outflow morphology

Figure 2 shows a channel map of the merged PdBI+30 m CO emission in IRAS 19410+2336, and we find a multitude of different features. Based on the channel maps the velocity-regimes of outflowing gas are defined as: blue wing [5–18] km s^{-1} and red wing [26–47] km s^{-1}. The velocity spread does not vary significantly for the different sub-outflows described below.

Comparing the single-dish CO emission presented in Fig. 1 with the high-resolution outflow map of the PdBI (Figs. 3a and 3b) we see that the overall structures in both datasets are similar, we just observe – as expected – much more structure in the interferometric data. Identifying the same structures makes us confident that the data reduction and merging process has been done properly, but the sub-structures demand a different morphological interpretation of the molecular outflows. Additionally, the near-infrared shocked H_2 data show many emission knots associated with the star-forming region (Fig. 3). Most of the H_2 features can be correlated with the molecular gas, but for some H_2 knots this is less obvious.

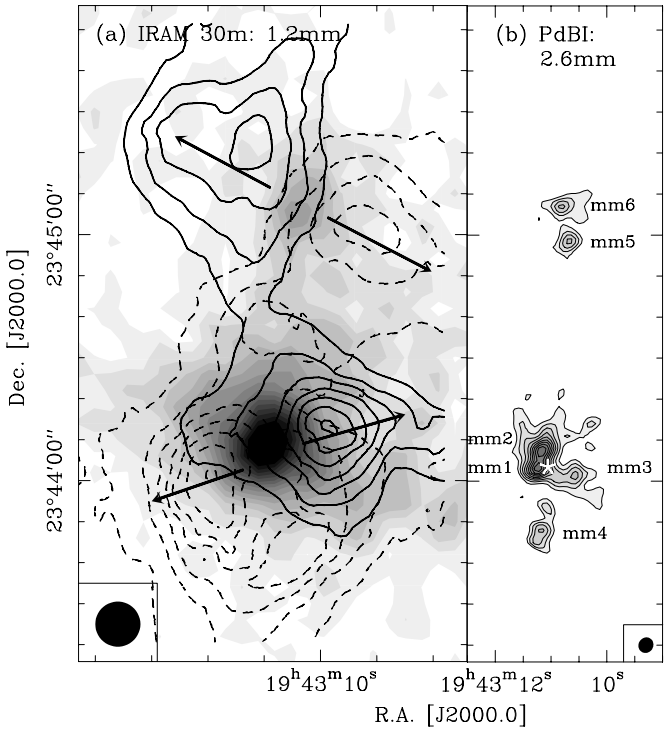

Fig. 1. The **left** panel presents the single-dish observations already published in Beuther et al. (2002b). In grey-scale we show the 1.2 mm dust emission, and the solid and dashed contours outline the blue and red CO(2–1) outflow emission. Both datasets were observed with the IRAM 30 m telescope at a spatial resolution of 11″ (bottom left). The arrows mark the two outflows identified previously from these observations. In the **right** panel, we present the PdBI 2.6 mm continuum data and label the sub-sources. The beam is presented at the bottom right and the white cross marks the position of the cm continuum source.

We identify four molecular outflows in the southern core and three outflows associated with the northern core. The identifications of the outflows are not unambiguous, and we are still resolution limited. Therefore, we note that the identifications below are just one interpretation, others might be possible and only very-high-spatial-resolution observations anticipated for next winter will clarify the picture.

3.2.1. The southern region

The morphological interpretation of the four southern outflows is sketched in Figs. 2 and 3.

South (A): the structures labeled (A) and (B) could also be part of only one outflow, but combining the CO and H_2 observations this does not seem likely and we prefer the interpretation of two different overlapping outflows. The outflow South (A) corresponds to the main large scale outflow already identified in the single-dish observations (see Figs. 1–3). It runs in east-west direction and is centered approximately on the main southern sub-core mm1 which also houses the cm-source and the maser emission. Morphologically, one of the X-ray sources could also be the center of the outflow, but the main mm source seems to be more likely.

South (B): the H_2 features (1, 4–6) and the corresponding CO emission outline the ellipsoidal structure of outflow South (B) sketched in Figs. 2 and 3. As the molecular emission at the eastern end of the outflow has a strong gradient and stops rather instantaneously directly before the H_2 feature (1), it is likely that both – CO and H_2 – outline a bow-shock-like working surface between an underlying jet and the surrounding molecular gas. The mm source mm3 likely houses the driving source of outflow South (B). As discussed below, the H_2 features (4), (5) and (6) might outline the interface between the outflow cavities of outflow (B) and the northern outflow (F).

South (C): the third southern outflow (C) is virtually undetectable in the single-dish data because it is very small in extent but clearly resolved in east-west direction in the high-resolution PdBI data. The elongated H_2 emission feature (2) is strongly associated with the blue molecular gas and outlines the same morphological structure, indicating a highly collimated outflow. The H_2 knot (3) is at the eastern end of the red CO gas and can be part of this outflow as well. South (C) is near the center of the region and might also be driven by the mm source mm1 or another source nearby. With the current spatial resolution it is likely that the outflows South (A) and (C) emanate from the same mm continuum condensation. At a distance of 2.1 kpc, the beam-size of 3.9″ × 3.6″ corresponds to a linear resolution of approximately 7900 AU. Thus, it is well possible that a multi-component system is evolving within mm1 and the outflows emanate from different members of the system similar to observations in, e.g., HH288 (Gueth et al. 2001) or IRAS 05358+3543 (Beuther et al. 2002d).

South (D): the fourth southern outflow labeled (D) is further to the west and runs roughly north-south. It would already have been possible to identify this flow in the single-dish data, but this structure does not stand out prominently there (Fig. 1). We do not find a mm continuum or X-ray source at the center of this outflow (Figs. 2 and 3). The driving source can well be hidden in the noise because the continuum mass sensitivity is >20 $M_\odot$ (Sect. 3.1). The H_2 feature (3) is in the vicinity of this outflow but we cannot unambiguously attribute it to South (C) or (D).

3.2.2. The northern region

The northern region has a similarly complex morphological structure and we suggest that at least three outflows are present there.

North (E): as for the outflows South (A) and (B), the northern outflows (E) and (F) could also be parts of only one outflow system, but for those structures, especially the CO emission indicates the existence of two overlapping outflows. Outflow North (E) runs in a collimated way roughly in east-west direction and corresponds to the previously detected single-dish outflow in this region. Likely, the mm source mm5 is the driving source of this outflow.

North (F): while the single-dish data suggested a simple morphology (Fig. 1), the red emission between the northern and southern core stands out far more prominently in the PdBI data. Therefore, we suggest that the red emission

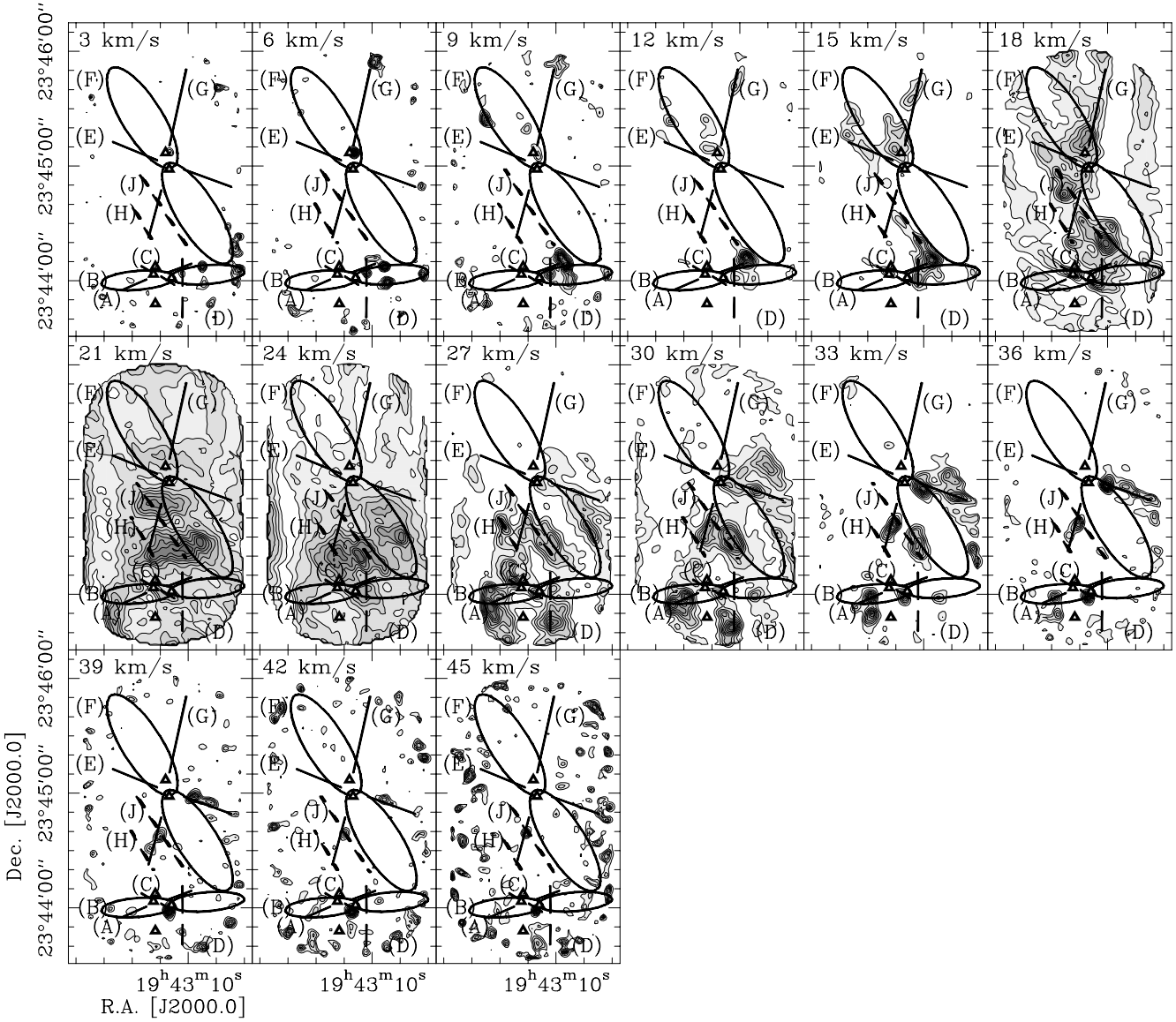

Fig. 2. Channel map of the merged PdBI and 30 m CO(1–0) observations. The data are binned into 3 km s^{-1} channels and labeled each at the top-left. The arrows, ellipses, letters and markers outline the outflows and mm sources (triangles) as discussed in the text.

outlines the ellipsoidal walls of a cavity-like outflow, as outlined in Figs. 2 and 3. The blue-shifted emission to the northeast shows a cavity-like structure as well and supports this interpretation. In Fig. 2, the cavity structures are best observed at velocities 18, 30, 33 km s^{-1}. In this picture, the H_2 features (4), (5) and (6) indicate shocked gas at the interface between the cavities of the outflows (B) and (F). There is also a faint H_2 emission patch (12) in the north which could be part of the northern cavity and which is just outside our observed PdBI mosaic. The morphology suggests that the driving source of outflow (F) is located within the mm source mm5 but it could also be driven by mm6.

North (G): the finger-like blue filament pointing north has a a red counterpart pointing south, both centering around the mm source mm6. This morphology suggests a seventh outflow (G) running north-south. Source mm6 is approximately at the center of this structure and the only mm source where we find high-velocity gas as well as H_2 emission (10) centered on (Figs. 2 and 3). This suggest that the H_2 feature is directly produced from the underlying high-velocity jet. At the northern tip, we find weak H_2 emission (11) which can be associated with the blue CO emission. Due to the spatial overlap with other outflows, it is not clear how far south this North (G) proceeds and which part of the emission belongs to North (G) or rather to South (A), (B) and (C). There are more H_2 emission knots (7, 8, 9) associated with the southern part of this structure, but those features are difficult to interpret and it is not clear whether they are part of North (G) or belong to a completely different structure as outlined below.

3.2.3. Further tentative outflow structures

In the interface region between the northern and the southern core, we find red/blue CO emission and the H_2 features (7), (8), and (9).

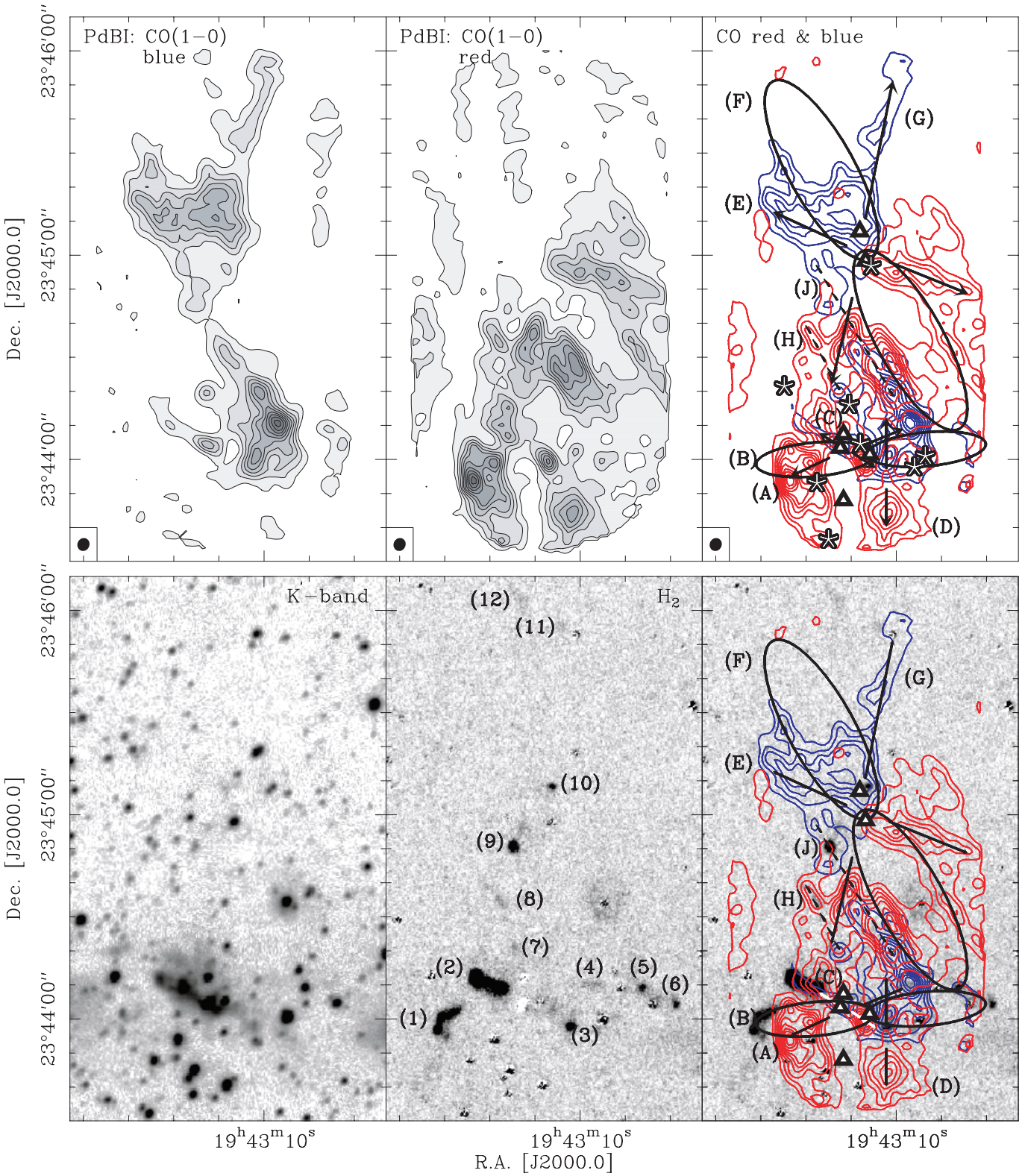

Fig. 3. Top: the left and middle panel show the blue (v[5–18] km s^{-1}) and red (v[26–47] km s^{-1}) CO emission separately (merged PdBI and 30 m data). The right panel then presents the combined outflow emission and marks the outflows (arrows, ellipses and letters), mm sources (triangles) and X-ray sources (stars) as discussed in the text. **Bottom:** the left and middle panels show the K' and H_2 images from Calar Alto, respectively. The labels in the middle panel mark the H_2 features discussed in the text. The contours in the right panel again show the PdBI CO emission, this time as an overlay on the H_2 map. The markers and errors are the same as in the top panel.

While it is possible that (7) and (8) are produced by outflow North (G), the elongated H_2 emission (7) coincides with elongated red CO emission. Additionally, Fig. 3 shows blue CO emission at the H_2 knot (7). These observations allow the tentative detection of another outflow (H) outlined by the dashed line in Fig. 3. We do not detect a mm continuum source there as the outflow driver, but, as already mentioned, the continuum sensitivity corresponds only to a mass sensitivity of >20 $M_\odot$, and a low-mass source can easily be hidden there.

In addition to the red CO emission corresponding to outflow North (F), there is also strong blue CO emission at the interface of the northern and the southern star-forming cores. It is not entirely obvious where this structure belongs to, but its north-east to south-west elongation, the associated red CO emission and the H_2 knot (9) suggest that even a ninth outflow (J) might be depicted by these structures. There is no mm source detected in that region as well. We stress that the structures (H) and (J) are even more ambiguous than the other seven outflows discussed before. Higher spatial resolution and sensitivity are needed to derive a conclusive picture of the different outflow phenomena.

3.3. Position–velocity diagrams

In spite of the seemingly chaotic morphology, the data still allow a kinematic interpretation. Therefore, we present in Fig. 4 position–velocity diagrams for the five non-ellipsoidal outflows (A, C, D, E, G) as well as for the tentative structures (H) and (J). North (G) is the only outflow with high-velocity gas at its center, for the other outflows, the velocities increase with distance from the outflow center. This is also the case for the position velocity diagrams corresponding to (H) and (J), which is an additional indication that those features are part of outflows. The position–velocity morphologies resemble a Hubble-law, which can be interpreted due to the combination of momentum conservation of the protostellar winds and density decreases away from the driving sources of the outflows (e.g., Shu et al. 1991). Hydrodynamic jet-entrainment models also result in Hubble-like position–velocity diagrams (e.g., Smith et al. 1997; Downes & Ray 1999). The observed position–velocity diagrams resemble those known from low-mass star formation. It has to be noted that already the position–velocity diagrams derived from the single-dish data show similar features.

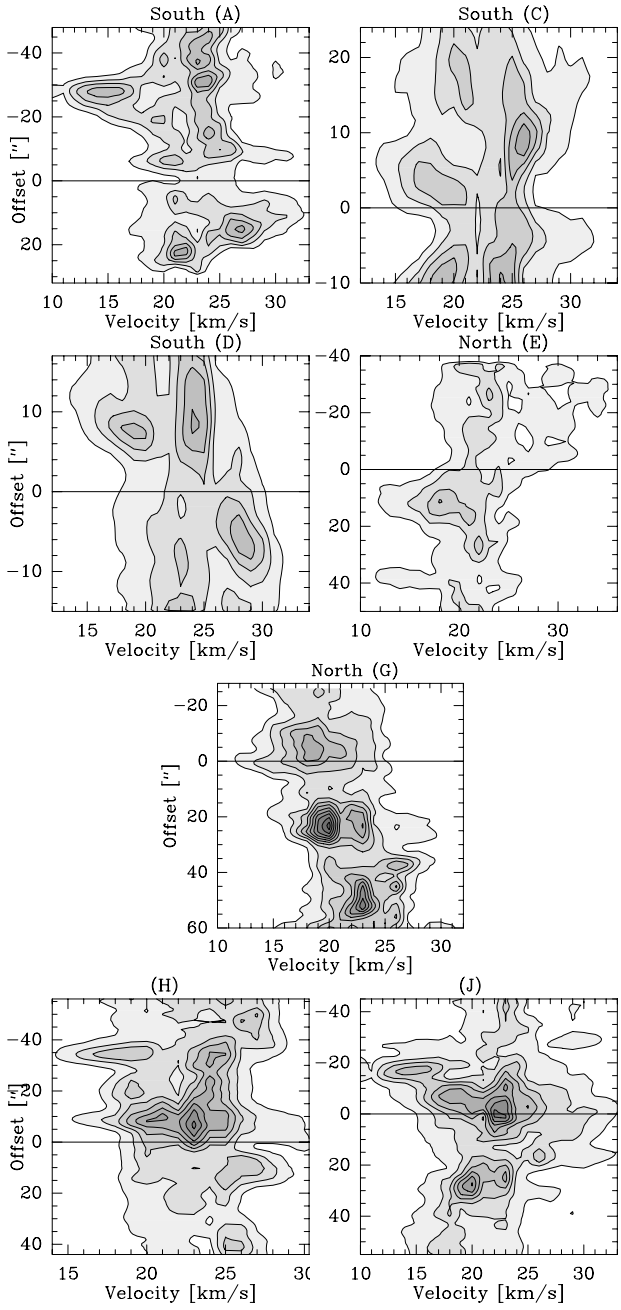

Fig. 4. Position–velocity diagrams for the five non-ellipsoidal outflows plus the two tentative ones (H) and (J). The horizontal line in each diagram corresponds to the anticipated outflow center. The latter are only assumptions for (H) and (J).

3.4. Outflow parameters

In addition to morphological and kinematic interpretations, we estimate masses, energetics and outflow rates of the individual sub-flows. Because there is significant overlap between the various outflows, often we cannot distinguish how much emission corresponds to one or another of the overlapping outflows. Thus, some emission features are used to derive the parameters for different outflows. In the following, we present the outflow parameter for the single-dish observations (Beuther et al. 2002b), compare them with the outflow parameters derived for the same regions from the merged PdBI and 30 m data, and finally discuss the outflow characteristics of the individual sub-outflow. It has to be noted that the single-dish results presented here deviate from the parameters presented in Table 2 of Beuther et al. (2002b), because in the former paper we erroneously derived the mass in the red outflow wing of IRAS 19410+2336 (south) using a wrong source size. This error occured only in this case, and the other parameters of Table 2 in Beuther et al. (2002b) are correct.

Opacity-corrected H_2 column densities N_b and N_r in both outflow lobes can be calculated by assuming a constant $^{13}CO/^{12}CO$ 1 – 0 line wing ratio throughout the outflows

Table 2. Outflow results: masses M_b (blue), M_r (red) and M_{out} ($M_{out} = M_b + M_r$) [$M_\odot$], momentum p [$M_\odot$ km s^{-1}], energy E [10^{46} erg], size [pc], time t [10^4 yr], mass entrainment rate $\dot{M}_{out}$ [10^{-4} $M_\odot$ yr^{-1}], mechanical force F_m [10^{-3} $M_\odot$ km s^{-1} yr^{-1}] and mechanical luminosity L_m [$L_\odot$].

source	M_b	M_r	M_{out}	p	E	size	t	$\dot{M}_{out}$	F_m	L_m
Single-dish observations with the IRAM 30 m in CO(2–1)										
South	11.2	19.8	31.0	683	1.5×10^{47}	0.4	19 510	1.6×10^{-3}	3.5×10^{-2}	63
North	11.2	13.4	24.6	541	1.2×10^{47}	0.5	20 420	1.2×10^{-3}	2.7×10^{-2}	49
Merged PdBI and single-dish data of the single-dish regions in CO(1–0)										
South	8.2	10.4	18.6	651	2.6×10^{47}	0.4	12 790	1.5×10^{-3}	5.1×10^{-2}	167
North	9.3	14.8	24.1	880	3.6×10^{47}	0.5	13 380	1.8×10^{-3}	6.6×10^{-2}	222
Merged PdBI and single-dish data of the individual outflows in CO(1–0)										
South (A)	2.6	3.0	5.6	192	7.6×10^{46}	0.3	8330	6.7×10^{-4}	2.3×10^{-2}	75
South (B)	1.7	1.6	3.3	107	4.1×10^{46}	0.4	11 300	2.9×10^{-4}	9.5×10^{-3}	30
South (C)	0.6	0.7	1.3	46	1.8×10^{46}	0.2	5060	2.6×10^{-4}	9.0×10^{-3}	29
South (D)	1.6	2.6	4.2	153	6.3×10^{46}	0.2	5950	7.1×10^{-4}	2.6×10^{-2}	87
North (E)	3.5	4.2	7.7	265	1.1×10^{47}	0.4	11 300	6.8×10^{-4}	2.3×10^{-2}	76
North (F)	4.5	8.1	12.6	472	2.0×10^{47}	0.6	17 840	7.1×10^{-4}	2.6×10^{-2}	91
North (G)	1.9	6.8	8.7	359	1.6×10^{47}	0.6	16 950	5.1×10^{-4}	2.1×10^{-2}	77

(Cabrit & Bertout 1990). Choi et al. (1993) found an average ^{13}CO/^{12}CO 2 – 1 line wing ratio around 0.1 in 7 massive star-forming regions, , corresponding to a $\tau(^{13}\mathrm{CO}\ 2-1) = 0.1$. We adopt this value for IRAS 19410+2336 as well, and we assume 30 K as average temperature in the outflow. The mass of entrained gas M_{out}, the dynamical timescale t and the outflow rate $\dot{M}_{outflow}$ are calculated via:

$$M_{out} = (N_b \times \mathrm{size}_b + N_r \times \mathrm{size}_r)\, m_{H_2}$$
$$t = \frac{r}{(v_{max_b} + v_{max_r})/2}$$
$$\dot{M}_{out} = \frac{M_{out}}{t}$$

with size_b and size_r the sizes of the outflow lobes, m_{H_2}, the mass of the H_2 molecule, and v_{max_b} and v_{max_r} the maximum velocities observed in each line wing. A more detailed description how the outflow parameters are determined is given in Beuther et al. (2002b). According to Cabrit & Bertout (1990) derived masses are accurate to a factor 2 to 4, whereas the accuracy of dynamical parameters are lower, at about a factor 10.

The first two sections of Table 2 correspond to the derived total outflow masses for the single-dish data and the merged PdBI data, respectively. The chosen outflow region is based on the single-dish data. Comparing the masses of entrained gas M_{out} from the single-dish and the PdBI observations, we find that the merged interferometric data compare reasonably well with the single-dish results. This approximate agreement is further support that the merging of the interferometric and single-dish data, and also their relative weighting, has worked properly. Additionally, it indicates that single-dish observations are adequate to derive global outflow properties.

More interesting are the parameters of all the sub-outflows derived separately. We note that summing up the values from all southern and northern outflows does not result in the total mass derived before, because the morphologies vary too much: e.g., some emission features believed from the single-dish data to be part of the southern flows belong in fact to different flows of the northern region. Furthermore, other emission patches are used to derive the parameters for different outflows because we cannot always distinguish unambiguously where they primarily belong to.

The derived outflow masses M_{out} are between 1 $M_\odot$ for the smallest outflow South (C) and 12 $M_\odot$ for North (F). The outflow rates are high, of the order a few times 10^{-4} $M_\odot$ yr^{-1}. Assuming momentum driven outflows, a velocity ratio between the entrained gas and the underlying jet of approximately 1/20 and a ratio between the jet-mass-loss rate and the accretion rate of 0.3, such outflow rates result in accretion rate estimates of the order 10^{-4} $M_\odot$ yr^{-1} (for details on the assumptions see Beuther et al. 2002b). Accretion rates of that order are necessary to overcome the radiation pressure and form massive stars via disk-mediated accretion processes (Stahler et al. 2000). The accuracy of mass, age and other parameters is not good enough to compare individual properties between the different flows in a meaningful way.

4. Conclusions

The new high-spatial resolution CO and H_2 observations of the high-mass star-forming region IRAS 19410+2336 resolve at least seven (possibly even nine) bipolar outflows. The large number of outflows and their interactions are an excellent example for the complexity in high-mass star formation. The data

show that the single-dish observations simplify the morphological picture of the region, but nevertheless give a good global picture of the region. Unfortunately, we also find that even the present interferometric spatial resolution is not sufficient to clearly disentangle the multiple overlapping outflows, different interpretations for some of the features are well possible. CO and H_2 emission mostly trace different parts of the same outflows, but it is not always possible to attribute all observational features unambiguously within the same interpretation. We note that here we present the – from our point of view – most plausible interpretation of the outflow morphologies, but it is well possible that follow-up observations will result in partly different outflow identifications because of the complexity of the region. Nevertheless, the whole picture is very suggestive of a scenario, where the global outflow properties of massive star-forming regions are a superposition of many different outflows emanating from the evolving massive cluster.

The masses and energetics of each sub-flow are, as expected, below the values derived from the single-dish data. Previous studies of other massive molecular outflows have also shown multiple outflows but the regions were dominated energetically by the most massive outflow (e.g., IRAS 05358+3543, Beuther et al. 2002d; IRAS 23033+5951, Wyrowski et al. in prep.). This is less clear in the case of IRAS 19410+2336: the northern core is dominated by outflow (F), but it does not seem to be the case as much in the south, (A) contributes only approximately 30% of the mass estimated for the whole southern core. The difference is lower if outflows (A) and (B) were not two, but are different parts of only one flow. However, this question cannot be resolved by the present observations. Combining the observations from the literature with these new data, we find that global core statistics based on single-dish observations are often valid, but the averaging aspect of the single-dish data has to be kept in mind.

Accretion rate estimates based on the outflow energetics are in the $10^{-4}\ M_{\odot}\,\mathrm{yr}^{-1}$ regime. Accretion rates of that order are important to overcome the radiation pressure of the forming massive stars, and thus build up the most massive objects via a continuous disk-accretion process.

Of additional interest are the position–velocity diagrams, which resemble a Hubble-like distribution as often reported in low-mass star formation (e.g., Smith et al. 1997; Downes & Ray 1999). This result is different to findings based on CO single-dish observations from Ridge & Moore (2001) who report that they do not find Hubble-like position–velocity dependence in any of their 11 studied massive outflow sources. In contrast, resolving the two single-dish outflows of IRAS 19410+2336 into at least seven outflows with the PdBI indicates that the kinematics of the individual outflows resemble the features known from low-mass star formation. Furthermore, the H_2 emission associated with South (C) suggests the presence of outflows in a well-collimated jet-like manner, as is found in low-mass protostars. Together, this is further support to the hypothesis that the physical processes in high-mass star formation are qualitatively similar to those found in their low-mass counterparts, the main difference being the clustered mode of formation and higher accretion and outflow rates (e.g., McKee & Tan 2003; Maeder & Behrend 2002; Beuther et al. 2002b,d).

Concerning the dust continuum emission, in our previous single-dish 1.2 mm observations with a spatial resolution of 11″, we found that the power-law density distribution does not continue to the very center, and we derived an inner breakpoint at 5″ for the southern core from where on we modeled the density distribution as flat (Beuther et al. 2002a). We suggested that this flattening is due to fragmentation of the large-scale core into many sub-sources. The new interferometric data directly confirm this hypothesis, and we observe the fragmentation into sub-cores (Fig. 1). The spatial separation of, e.g., mm1 and mm2 is ∼5″.

To summarize, the presented observations show the complex interaction of several molecular outflows within the massive star-forming region IRAS 19410+2336. In spite of the complexity, the analysis of the data supports the idea of massive star formation taking place in a clustered mode by similar physical processes as known for low-mass star formation, involving accretion through disks producing collimated outflows.

Finally, we note that follow-up observations of this region are necessary to understand the interplay of many molecular outflows within one star-forming region more properly. In spite of the similarity to low-mass star formation, the feed-back processes between many protostars in a high-density environment should also produce significant differences, IRAS 19410+2336 can be used as a template region for such studies. Regarding molecular outflows, different molecular observations are needed, especially interesting is SiO which is known to be a shock and jet tracer. Furthermore, we are still resolution limited, and it will be crucial to re-observe the region in CO(2–1) with significantly higher spatial resolution.

Acknowledgements. We would like to thank the IRAM Grenoble staff for the help during observations and data reduction, especially F. Gueth and D. Nürnberger. Additionally, we thank G. Paubert, the AoD at the 30 m telescope, for correcting the velocity information of the single-dish data offline. S. Bontemps helped resolving the distance ambiguity. H.B. acknowledges financial support by the Emmy-Noether-Programm of the Deutsche Forschungsgemeinschaft (DFG, grant BE2578/1).

References

Bally, J. 2002, in Hot star workshop III: The earliest stages of massive star birth, ed. P. A. Crowther, ASP Conf. Ser., 267
Beuther, H., Sridharan, T. K., Schilke, P., et al. 2002a, ApJ, 566, 945
Beuther, H., Schilke, P., Sridharan, T. K., et al. 2002b, A&A, 383, 892
Beuther, H., Walsh, A., Schilke, P., et al. 2002c, A&A, 390, 289
Beuther, H., Schilke, P., Gueth, F., et al. 2002d, A&A, 387, 931
Beuther H., Kerp, J., Preibisch, T., Stanke, T., & Schilke, P. 2002e, A&A, 395, 169
Bonnell, I. A., Bate, M., & Zinnecker, H. 1998, MNRAS, 298, 93
Cabrit, S., & Bertout, C. 1990, ApJ, 348, 530
Choi, M., Evans, N. J. II, & Jaffe, D. T. 1993, ApJ, 417, 624
Cesaroni, R., Felli, M., Testi, L., Walmley, C. M., & Olmi, L. 1997, A&A, 325, 725
Downes, T. P., & Ray, T. P. 1999, A&A, 345, 977

Gibb, A. G., Hoare, M. G., Little, L. T., & Wright, M. C. H. 2003, MNRAS, in press
Gueth, F., Guilloteau, S., & Bachiller, R. 1996, A&A, 307, 891
Gueth, F., Schilke, P., & McCaughrean, M. 2001, A&A, 375, 1018
Guilloteau, S., Delannoy, J., Downes, D., et al. 1992, A&A, 323, 943
Hildebrand, R. 1983, QJIRS, 24, 267
Hunter, T., Churchwell, E., Watson, C., et al. 2000, AJ, 119, 271
Jijina, J., & Adams, F. 1996, ApJ, 462, 874
Maeder, A., & Behrend, R. 2002, in Hot star workshop III: The earliest stages of massive star birth, ed. P. A. Crowther, ASP Conf. Ser., 267
McKee, C. F., & Tan, J. C. 2003, ApJ, 585, 850
Norberg, P., & Maeder, A. 2000, A&A, 359, 1025
Richer, J., Shepherd, D., Cabrit, S., Bachiller, R., & Churchwell, E. 2000, in Protostars & Planets IV, ed. V. Mannings
Ridge, N. A., & Moore, T. J. T. 2001, A&A, 378, 495
Schultz, A. S. B., Colgan, S. W. J., & Erickson, E. F. 1999, ApJ, 511, 282
Shu, F. 1977, ApJ, 214, 488
Shu, F., Ruden, S. P., Lada, C. J., & Lizano, S. 1991, ApJ, 370, L31
Smith, M. D., Suttner, G., & Yorke, H. 1997, A&A, 323, 223
Stahler, S., Palla, F., & Ho, P. 2000, in Protostars & Planets IV (The University of Arizona Press)
Shepherd, D., & Churchwell, E. 1996, ApJ, 457, 267
Shepherd, D. S., Watson, A., Sargent, A., & Churchwell, E. 1998, ApJ, 507, 861
Shepherd, D. S., Yu, K. C., Bally, J., & Testi, L. 2000, ApJ, 535, 833
Sridharan, T. K., Beuther, H., Schilke, P., Menten, K., & Wyrowski, F. 2002, ApJ, 566, 931
Wolfire, M. G., & Cassinelli, J. P. 1987, ApJ, 319, 850
Yorke, H. W., & Sonnhalter, C. 2002, ApJ, 569, 846
Zhang, Q., Hunter, T. R., Brand, J., et al. 2001, ApJ, 552, 167
Zinnecker, H., & Bate, M. R. 2002, in Hot star workshop III: The earliest stages of massive star birth, ed. P. A. Crowther, ASP Conf. Ser., 267